Proceedings of The Joint Canadian Society for Mechanical Engineering and CFD Society of Canada International Congress 2019
CSME-CFDSC Congress 2019
June 2-5, 2019, London, Ont, Canada

Experimental characterization of anisotropic mechanical properties of extruded AA6061-T6

M. Bondy, W. Altenhof*, J. Magliaro**
Mechanical, Automotive, and Materials Engineering
University of Windsor, Windsor, ON, Canada
*altenh1@uwindsor.ca **presenting author

M. R. Jensen
Certasim LLC
Saratoga, CA, USA
morten@certasim.com

ABSTRACT— An aluminum extrusion of a practical geometry for automotive crashworthiness applications was acquired for both mechanical testing of the geometry and material characterization from extracted specimens. The purpose of this endeavor was to collect data on the anisotropic mechanical properties resulting from the extrusion process. In terms of uniaxial tension data, there was a 3 % difference in yield stress between 0° (extruded direction) and 90° with 2 % coefficient of variation. However, plastic strain ratios were distinct in the 0°, 45°, and 90° directions with average plastic strain ratios of 0.51, 0.23, and 1.43, respectively. The German Automotive Industry Association (Verband der Automobilindustrie or VDA) *VDA 238-100* plate bending tests were distinct in terms of their force-deflection responses after the onset of failure, following development of the peak load, for all directions considered (0°, 15°, 30°, 45°, and 90°). Force responses after the onset of significant plastic deformation were distinct for 0°, 15°, and 30° specimens but essentially identical for 45° and 90°. Repeatable force-deflection and failure mechanisms were observed for three point bending of an aluminum extrusion of a practical geometry for automotive crashworthiness applications. Three-dimensional deflection data was acquired by digital image correlation to allow rigorous finite element model validation.

Keywords: aluminum; extrusion; anisotropy; failure; fracture

I. INTRODUCTION

Between 1985 and 1995 the mass of aluminum in an average automobile in Western Europe, Japan, and North America increased by approximately 30% with the expectation that this trend would accelerate over the next 10 years [1]. Over a similar duration of time it has been observed that total vehicle mass has increased by approximately 17% [2]. A trend has been observed in the automotive industry where lightweight materials became economically viable and were implemented when costs dropped below $4.50 USD per kilogram of mass reduction ($2.00 USD per pound) [3]. Aluminum has traditionally been implemented in enclosures (e.g. front hoods, trunk lids, door panels) at a cost of $4.00 USD per kilogram. More recently, aluminum-bodied vehicle chassis and body components have been mass produced, such as the 2015 Ford F-150 and Tesla Model S bodies, and the chassis of the 2016 Jaguar XE.

Before novel, lightweight materials can be employed to reduce vehicle mass, the mechanical performance (i.e. crashworthiness, durability, and noise/vibration/harshness) of a vehicle must be maintained or exceeded. Motor vehicle collisions in Canada resulted in over 2000 fatalities, 160 000 ER visits, and 170 000 injuries in 2010 at a cost of $2.2 Billion [25]. For stiff alloys, with maximum strength for structural applications, accurate predictions of material failure are critical for numerical modelling in the field of vehicular crashworthiness. Furthermore, it has been shown that for a plethora of materials, the accuracy of a numerical model may be strongly influenced by the manufacturing process due to significant anisotropy between mechanical properties. Therefore, this study was postulated to achieve the following:

- Mechanically characterize a commercially available, 6061-T6 aluminum extrusion at large deformations applying standardized testing methodologies.
- Complete material characterization on standardized specimens extracted from this extrusion at multiple orientations with respect to the extruded direction.
- Employ digital image correlation (DIC) to acquire high resolution displacement fields from extrusions subjected to three point bending for comprehensive finite element model validation.

II. LITERATURE REVIEW

Numerous publications exist documenting experimental characterization and modelling of the failure and anisotropy of aluminum alloys. Luo et al. [4] acquired surface strain fields and load-deflection data for tensile specimens with notches and with a central hole, and butterfly shear specimens for 6260-T6 sheets (2 mm thickness). Novel yield [5] and fracture models were proposed and implemented in ABAQUS with the capability to accurately capture the onset of fracture for all specimen configurations. Wadley et al. [6] developed a finite element model of an extruded 6061-T6 sandwich panel subjected to blast loading. Tensile tests were completed for three orientations: 0° (extruded direction), 45°, and 90°. Significant variation between tests with the consistent specimen orientations was observed. The Johnson and Cook [7] isotropic constitutive equation was utilized for the relationship between effective plastic strain and effective stress. Failure was predicted with the isotropic Cockroft-Latham failure model [8].

A detailed investigation of the anisotropy of AA6061-T6 sheets was published by Beese et al. [9]. Several specimen configurations, including but not limited to tensile tests and butterfly shear specimens, were employed to obtain failure strain as a function of stress triaxiality in the range of -0.2 to 0.7. Fracture strains at the specimen surface were measured with DIC software. Average fracture strains were determined from thickness reductions while local fracture strains were estimated through an inverse method employing finite element models. Anisotropy due to the process of rolling, drawing and/or extruding a metallic is a well-documented phenomenon, starting with the work of Hill [10], [11] and followed by enhancements in the theory for states of plane stress by Barlat et al. [12]. The metals were shown to possess elongated grains in the extruded directions due to crystal plane realignment. Optical microscopy of AA6061-T6, square extrusions was performed by Jin [13] which investigated and confirmed the presence of these attributes for the alloy.

The influence of stress triaxiality on failure for AA6061-T6 has been investigated at the length scale of the grain structure by Ghahremaninezhad and Ravi-Chandar [14, 15]. Uniaxial tension, notched tension, and Arcan specimen, pure shear/superposed tension-compression experiments were completed with commercial and custom developed DIC software. The latter software extrapolated strain from grain deformation. For stress triaxialities in the ranges of -0.1 to 0 and 0.4 to 1, lower bounds on strain to failure were identified. The observed strain to failure was larger by almost an order of magnitude with respect to the predictions from the Johnson-Cook damage model identified by Lesuer et al. [16] for cross rolled AA6061-T6 plates.

The mechanisms for damage associated with ductile fracture are void nucleation, followed by their growth until coalescence between voids occurs [17, 18]. However, in a precipitate hardened alloy like 6061-T6, damage evolution is influenced by particle/inclusion size in addition to grain size. The earliest damage models were porous plasticity models accounting for the effect of void growth [19] and extended to include nucleation and coalescence [20, 21]. Phenomenological damage models are commonly found in commercial finite element software packages and range from continuum damage mechanics (CDM) models which consider statistical thermodynamics to models employing a damage indicator/parameter, *D* which is a function of the state of stress and/or strain. Two commonly utilized models of the latter category are the Johnson-Cook [7] and Cockroft-Latham [8] models.

The field of failure characterization for anisotropic metals is relatively novel with minimal standardized practices. VDA developed a test for assessing formability: *VDA 238-100: Plate bending test for metallic materials* [22]. This standardized test cannot replace the specimen configurations referenced previously while maintaining equal fidelity in terms of strain to failure as a function of stress triaxiality. However, in many industrial applications, the feasibility of material characterization can be limited by time and financial resources which may not permit the dependence of failure on both stress triaxiality and Lode parameter to be identified experimentally. Larour et al. [23] completed a sensitivity analysis of the VDA 238-100 test noting multiple factors which influenced the bending angle (e.g. elastic deformation of the apparatus and specimen curvature) and recommended this angle to be measured optically, since the equation in [22] to analytically compute the angle neglects the punch thickness which can result in errors of magnitudes up to 10%.

III. Methodology

A. Uniaxial tension testing

Uniaxial tension tests were completed for 9 specimens in each of the three orientations (0°, 45°, and 90° where 0° denotes a specimen where the load is applied in the extruded direction) for a total of 27 specimens. All specimens were extracted by wire electrical discharge machining (EDM) from one 6.1 m length of AA6061-T6 square tubing having a side length of 101.6 mm and wall thickness of 3.175 mm. Each set of specimens (3 at 0°, 45°, and 90°) were extracted from the ends and midspan of the extruded length. ASTM standard B557 [26] was followed for all uniaxial tension tests. A sub-sized specimen geometry was implemented given the 101.6 mm (4 inch) width of the extrusion. Tests were completed at a constant crosshead speed of 5 mm/min on a 50 kN MTS Criterion electromechanical load frame. For the elastic regime Poisson's ratio was acquired by post-processing the displacement field acquired with Correlated Solutions VIC-2D DIC software. Lankford coefficients (as functions of effective plastic strain) were similarly computed for plastic deformation . Each test was recorded by a 1.3 MP Allied Vision Manta monochrome camera with a Sill Optics S5LPJ5160 large working distance, high magnification lens at a frame rate of 17 fps. Poisson's ratio was calculated consistent with the procedure in ASTM standard D638. Lankford coefficients were computed consistent with ASTM E517.

B. VDA 238-100 Plate Bending Test for Metallic Materials

The numbers and orientations of specimens utilized for the VDA238-100 plate bending tests was consistent with the uniaxial tensile test methodology. Standard VDA specimens (60 mm by 60 mm) were extracted by wire EDM. A fixture consistent with the requirements of the VDA 238-100 standard was fabricated, as shown in Figure 1. A custom testing procedure was developed for the MTS load frame consistent with the VDA standard such that the crosshead speed was 10 mm/min until the 100 N preload, specified in the VDA 238-100 procedure, was observed. When this preload was achieved the load frame automatically increased the crosshead speed to 20 mm/min. Load-displacement data for both crosshead speed regimes were acquired but for post-processing, the punch displacement was set to zero at the 100 N preload. MTS Advantage video extensometer software, with identical camera hardware to that employed for the tensile tests, was utilized to track 12 points on the edge of the specimen and estimate the bending angle. For each set of 6 points, separated by the axis of the punch, a line fit using least squares regression was employed. These two lines were used to compute the bending angle as a function of punch displacement.

Figure 1. VDA 238-100 plate bending test setup.

C. *Three-Point Bending of an Aluminum Extrusion*

Three-point bending of 609.6 mm (24 inch) length, square extrusion with the previously mentioned profile dimensions was completed on a 150 kN MTS Criterion electromechanical load frame with an MTS 642.25 three-point bending fixture. The roller diameter of the three-point bending apparatus was 50.8 mm (2 inch) with a support spacing of 457.2 mm (18 inch). The extrusion had sharp corners; the radius was approximately 0.4 mm (measured with minimal precision using available radius gauges). The loading rate was 20 mm/min to a maximum crosshead displacement of 80 mm. The 3D displacement field on the surface of the specimen was acquired with two, 5 MP (2096 x 2048 pixels^2) Point Grey Research Grasshopper cameras equipped with Schneider-Kreuznach 30 mm lenses, and Correlated Solutions VIC-3D software. Images were captured with VIC-Snap from Correlated Solutions at a framerate of 1 fps. Synchronization of the load-deflection data and displacement field from DIC was accomplished by TTL signal state changes at one of the user-defined outputs of the MTS load frame to initiate and terminate image acquisition by the DIC system.

D. *Axial Compression of an Aluminum Extrusion*

Axial compression of 300 mm lengths of aluminum tubing was completed on a Tinius Olsen load frame. The force was measured with two, 220 kN load cells in parallel. Displacement was measured with an Acuity 300 mm non-contact laser displacement transducer. Both transducers were connected to a National Instruments CompactDAQ chassis with analog input modules and custom software developed in LabVIEW. The data was acquired at a rate of 3 kHz and the average crosshead displacement speed was approximately 16 mm/min.

IV. Results and Discussion

A. *Uniaxial tension tests*

Engineering stress-strain responses for 0° tensile specimen orientation are provided in Figure 2. The mean elastic modulus, Poisson's ratio, yield stress, tensile strength, and strain at failure are summarized in Table 1; the values in parentheses are coefficients of variation, expressed as percentages. As observed through analysis of data in Table 1, significant anisotropy was not observed in terms of the uniaxial stress-strain data (a 3.4% increase in yield stress was estimated from 90° to 0° with a coefficient of variation of approximately 2%). However, distinct responses between orientations were observed in terms of the plastic strain ratio, also known as R-values or Lankford coefficients. Lankford coefficients are plotted as a function of effective plastic strain in Figure 3 for the 0°, 45°, and 90° directions. Significant noise in the Lankford coefficient data necessitated post-processing by fitting a 6th-order polynomial to each averaged Lankford coefficient versus effective plastic strain response.

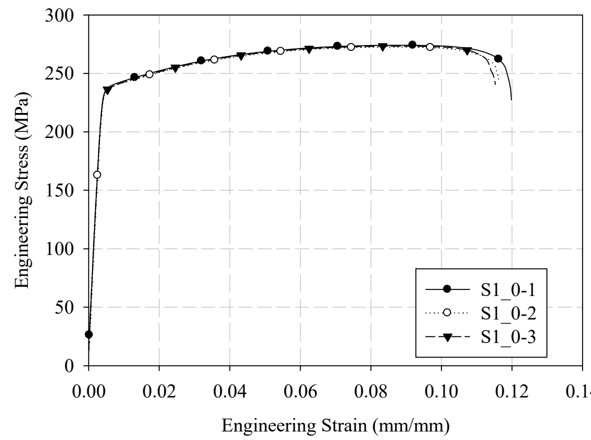

Figure 2. Uniaxial tensile stress-strain data, 0° specimens.

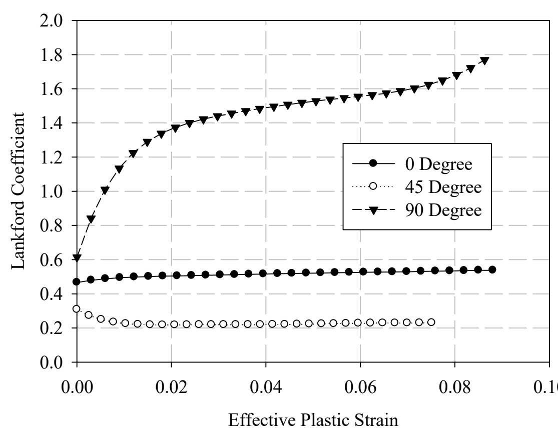

Figure 3. Lankford coefficients with respect to effective plastic strain.

TABLE 1. TENSILE DATA SUMMARY

	Modulus [GPa]	Yield Stress [MPa]	Ultimate Strength [MPa]	Strain at Fracture	Poisson's Ratio
0°	63.41 (1.93%)	247.3 (2.45%)	280.5 (1.81%)	0.118 (4.69%)	0.334 (10.2%)
45°	68.12 (1.03%)	246.2 (1.37%)	274.5 (0.85%)	0.098 (6.09%)	0.317 (9.19%)
90°	65.00 (1.57%)	239.1 (1.83%)	273.3 (1.60%)	0.113 (4.41%)	0.355 (6.81%)

B. *VDA 238-100 Plate Bending Test for Metallic Materials*

Force-deflection responses for the VDA plate bending tests are presented for the 0° orientation in Figure 4 to illustrate the consistency between tests of the same direction. To facilitate comparison with other mechanical data it is noted that the 0° specimen configuration was orientated consistent with the VDA standard such that the normal stress (bending) was in the normal direction. Distinct responses were observed to be functions of specimen orientation, particularly in terms of force-deflection responses beyond the peak load (i.e. onset and propagation of failure). However, the force-deflection responses were not identical between the onset of significant plastic deformation (approximately 0.75 mm of deflection) and the peak load. Considering micrographs presented in [24], there may be a skin-core grain structure resulting in this observation of anisotropy under bending but not under uniaxial tension, both in terms of plastic deformation and failure.

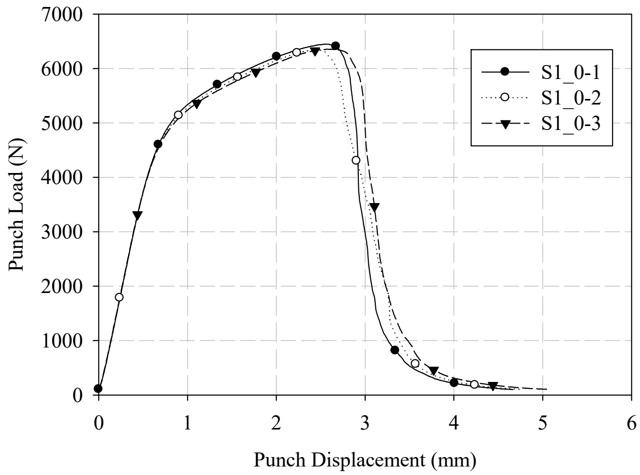

Figure 4. VDA force-deflection responses, 0° specimens.

Based upon the difference in pre-peak force behavior between 0° and both 45° and 90°, which exhibit similar force-deflection behavior prior to the onset of failure, additional directions were considered as shown in [5]. Where the orientation was the same, mechanical responses were near-identical to specimens characterized in the first round of testing. The mechanical behavior in the additional 15° and 30° orientations were consistent with the outlined expectations: the force-deflection responses progressively shift towards the behavior observed at the 45° orientation.

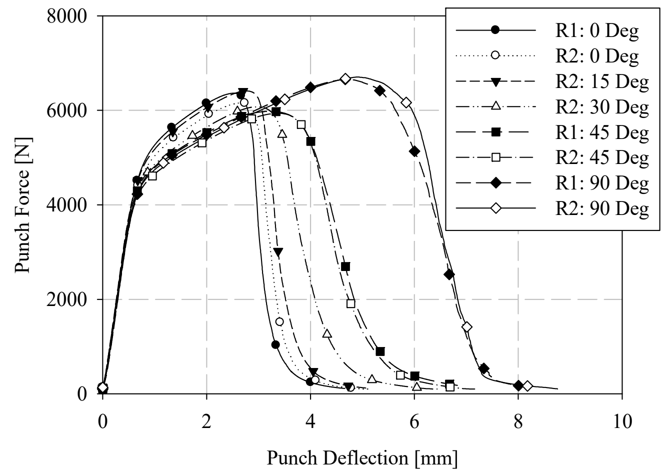

Figure 5. VDA force deflection responses at 0°, 15°, 30°, 45°, and 90°.

C. *Three Point Bending of an Aluminum Extrusion*

Force-deflection responses for the extrusions subjected to three-point bending are shown in Figure 6. All specimens were highly consistent in terms of their force-deflection responses and the failure location and propagation; fracture locations are shown in Figure 7. Significant bending and curvature at the failure locations is noted, indicating that the failure mechanisms of the VDA238 tests could assist with tuning a damage model for this application.

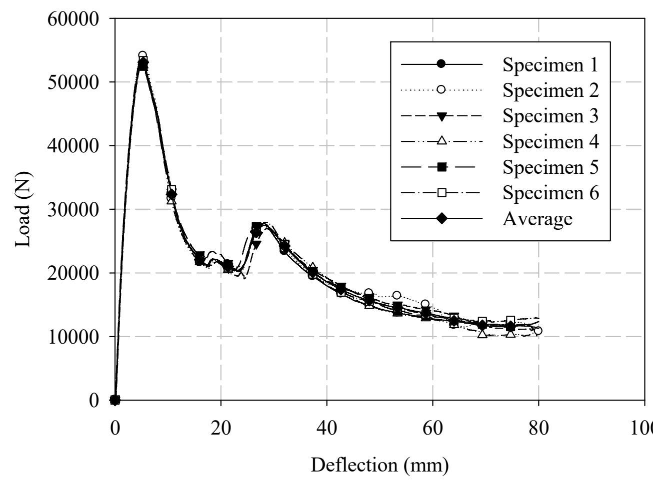

Figure 6. Force-deflection responses of three-point bending tests.

Figure 7. Repeatable failure/fracture at extrusion midspan (compressed surface in contact with midspan roller).

Deflection measurements (X, Y, and Z, respectively) from the DIC analyses for the extrusions subjected to three-point bending are presented in Figure 8 to Figure 10 for a crosshead displacement of 10 mm. Directions of the X and Y axes are illustrated in Figures 8 to 10 and applied for Figures 8 through 16. The Z axis direction is computed as the cross product of unit vectors in the X and Y directions. Deflections at a crosshead displacement of 20 mm are shown in Figure 11 to Figure 13 and for 30 mm deflections in Figure 14 to Figure 16. The projection error was less than 0.1 pixels for all data sets presented in this manuscript. Deflections in the X-direction exhibited the expected symmetry in terms of magnitude with reversal of direction across the plane of symmetry; Y- and Z-deflections were highly symmetric. Z-deflections (out-of-plane direction) were localized with respect to the cylindrical indenter.

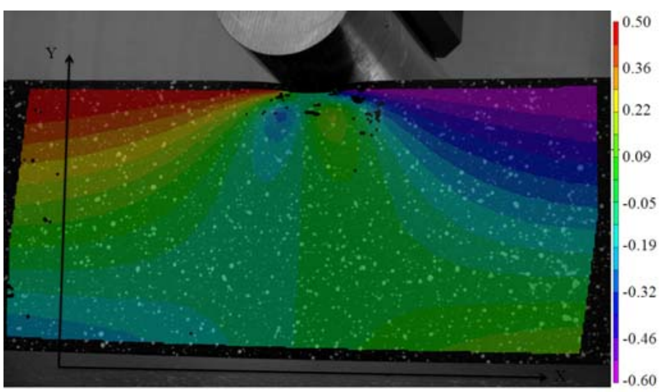

Figure 8. X-deflection [mm] at a crosshead displacement of 10 mm.

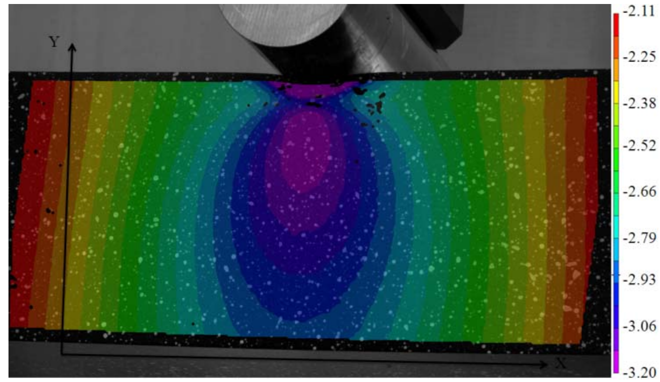

Figure 9. Y-deflection [mm] at a crosshead displacement of 10 mm.

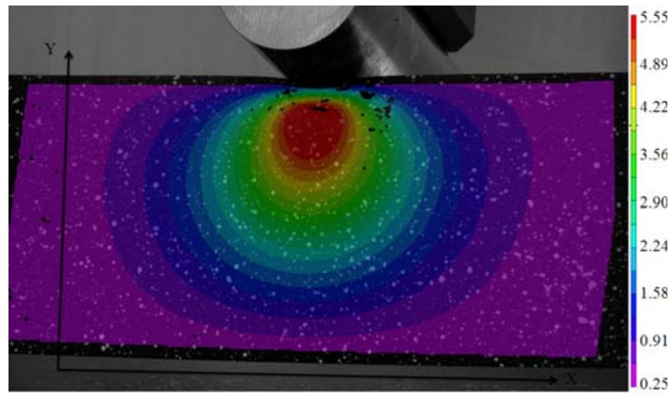

Figure 10. Z-deflection [mm] at a crosshead displacement of 10 mm.

Maximum deflections in the X-direction (longitudinal) increased proportionally (approximately 224%) more than the indenter displacement as indenter displacement doubled from 10 mm to 20 mm, as observed by comparing Figure 8 and Figure 11. Y-deflection doubled with a 100% increase in indenter displacement as noted by inspection of Figure 9 and Figure 12. Similar trends are observed when comparing Figure 11 to Figure 14 and Figure 12 to Figure 15.

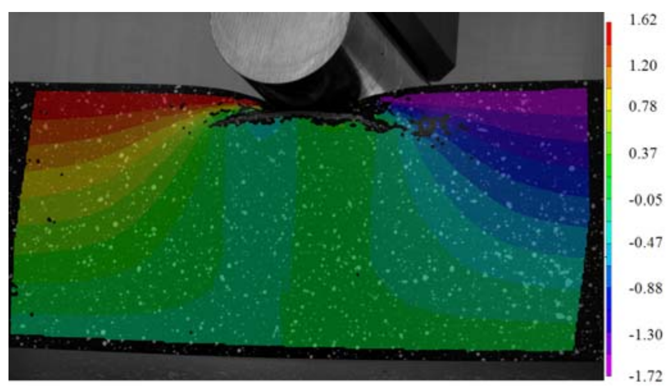

Figure 11. X-deflection [mm] at a crosshead displacement of 20 mm.

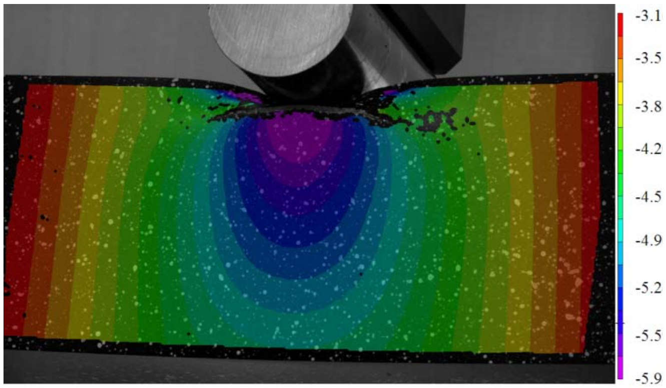

Figure 12. Y-deflection [mm] at a crosshead displacement of 20 mm.

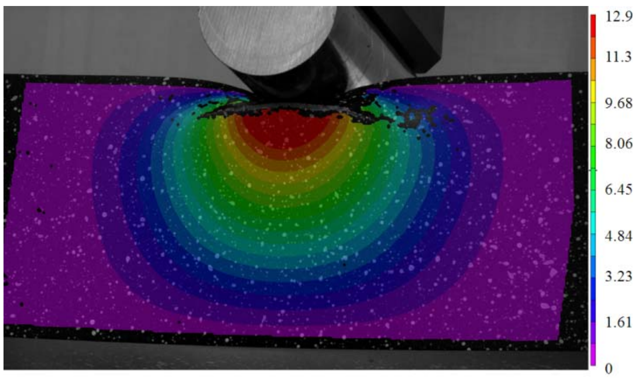

Figure 13. Z-deflection [mm] at a crosshead displacement of 20 mm.

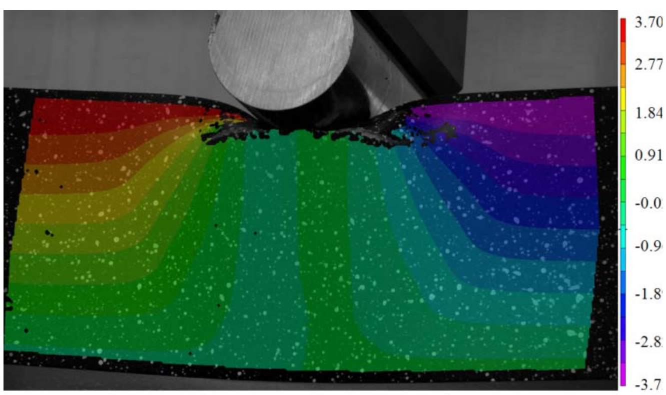

Figure 14. X-deflection [mm] at a crosshead displacement of 30 mm.

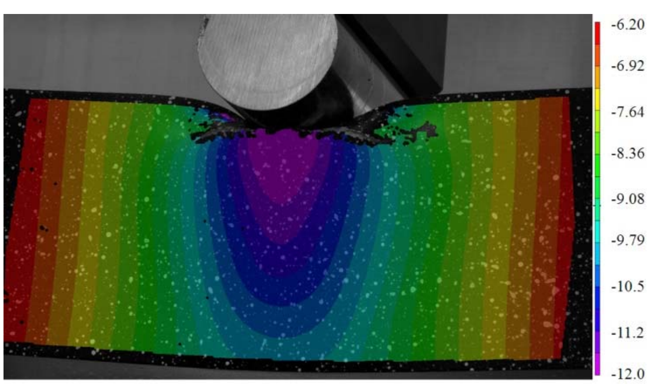

Figure 15. Y-deflection [mm] at a crosshead displacement of 30 mm.

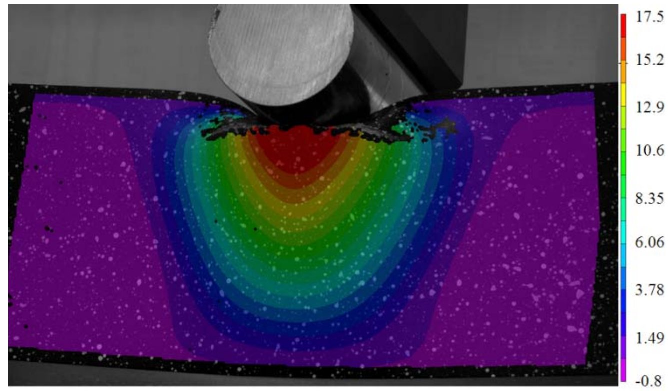

Figure 16. Z-deflection [mm] at a crosshead displacement of 30 mm.

D. *Axial Compression of Aluminum Extrusions*

Load-deflection responses for aluminum extrusions subjected to axial compression are given in Figure 17. The first 3 of 9 specimen responses are included in addition to an average of all 9 responses. All specimens post-test are shown in Figure 18. Most specimens buckled at or near their ends, however, a small number buckled approximately at the midspan. This did not significantly affect the load-deflection responses but presented challenges for use of the deflection fields acquired through DIC.

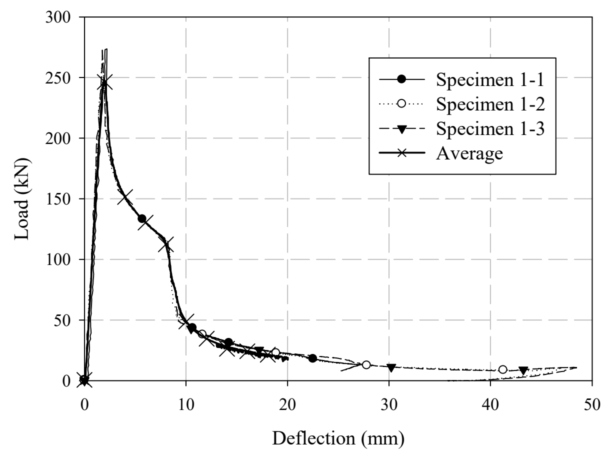

Figure 17. Force-deflection responses of axial crushing tests.

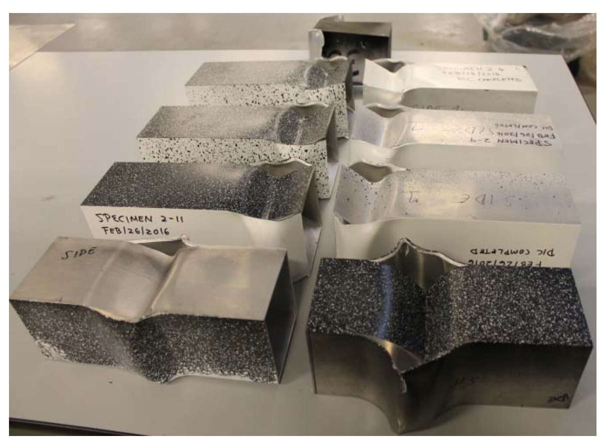

Figure 18. Specimens subjected to axial compression, post-test.

V. CONCLUSIONS & FUTURE WORK

Uniaxial tension tests did not exhibit anisotropy in terms of stress (a 3% difference in yield stress with 2% coefficient of variation was observed). However, plastic strain ratios were distinct in the 0°, 45°, and 90° directions. The average plastic strain ratios were 0.51, 0.23, and 1.43 for the 0°, 45°, and 90° orientations, respectively. VDA plate bending tests were unique in terms of their force-deflection responses after the onset of failure (peak load) for all the considered specimen orientations (0°, 15°, 30°, 45°, and 90°). Force-deflection responses after the onset of significant plastic deformation were distinct for 0°, 15°, and 30° specimens and near-identical for the 45° and 90° specimens. Repeatable force-deflection responses and failure mechanisms were observed for square aluminum extrusions, a practical geometry for automotive crashworthiness applications, subjected to three-point bending. Three-dimensional deflection data was acquired by digital image correlation to allow for rigorous finite element model validation in future investigations. Axial compression of 300 mm lengths of aluminum extrusion was also completed. While the force-deflection responses were consistent, the location at which buckling occurred varied between specimens.

This project was completed in partnership with CertaSim, a software distributor/support service provider for the finite element modelling software IMPETUS. One outcome was the enhancement of a Cockroft-Latham damage model to improve the fidelity of the anisotropy capabilities of the implementation of this damage model in IMPETUS. The previous version of this model included 2 parameters (0° and 90°). The revised implementation included a third parameter for the 45° orientation. Future work includes: finite element modelling of the three-point bending test documented here; mechanical testing of this extrusion under compressive loading (axial crush); and finite element modelling of axial crushing.

REFERENCES

[1] O. Hopperstad, B. Leira, S. Remseth, and E. Trømborg, "Reliability-based analysis of a stretch-bending process for aluminium extrusions." *Computers & Structures*, 1999. 71(1): p. 63-75.

[2] L. Chauvet, "Trelleborg Weight Reduction Strategy-Utilization of Plastic for Structural Components for Power Train Mounting System," 2012, *SAE Technical Paper* # 2012-28-0017.

[3] A. I. Taub and A. A. Luo, "Advanced lightweight materials and manufacturing processes for automotive applications." *MRS Bulletin*, 2015. 40(12): p. 1045-1054.

[4] M. Luo, M. Dunand, and D. Mohr, "Experiments and modeling of anisotropic aluminum extrusions under multi-axial loading–Part II: Ductile fracture." *Int. J. Plast.*, 2012. 32: p. 36-58.

[5] M. Dunand, A. P. Maertens, M. Luo and D. Mohr, "Experiments and modeling of anisotropic aluminum extrusions under multi-axial loading–Part I: Plasticity." *Int. J. Plast.*, 2012. 36: p. 34-49.

[6] H. N. Wadley, T. Børvik, L. Olovsson, J. J. Wetzel, K. P. Dharmasena, O. S. Hopperstad, V. Deshpande, and J. W. Hutchinson, "Deformation and fracture of impulsively loaded sandwich panels." *J. Mech. Phys. Solids*, 2013. 61(2): p. 674-699.

[7] G. R. Johnson and W. H. Cook, "Fracture characteristics of three metals subjected to various strains, strain rates, temperatures and pressures." *Eng. Fract. Mech.*, 1985. 21(1): p. 31-48.

[8] M. Cockcroft and D. Latham, "Ductility and the workability of metals." *J. Inst. Met.*, 1968. 96(1): p. 33-39.

[9] A. M. Beese, M. Luo, Y. Li, Y. Bai, and T. Wierzbicki, "Partially coupled anisotropic fracture model for aluminum sheets." *Eng. Fract. Mech.*, 2010. 77(7): p. 1128-1152.

[10] R. Hill, "A theory of the yielding and plastic flow of anisotropic materials." *Proc. Roy. Soc. A*, 1948. 93: p. 281–97.

[11] R. Hill, "Constitutive modelling of orthotropic plasticity in sheet metals." *J. Mech Phys.* Solids, 1990. 38(3): p. 405 – 417

[12] F. Barlat, Y. Maeda, K. Chung, M. Yanagawa, J.C. Brem, Y. Hayashida, D.J. Lege, K. Matsui, S.J. Murtha, S. Hattori, R.C. Becker, and S. Makosey, "Yield function development for aluminum alloy sheets" *J. Mech. Phys. Solids*, 1997. 45(11-12): p. 1727 – 1763

[13] S.Y. Jin, "Novel cutting deformation modes on axially loaded circular AA6061-T6 extrusions for superior crashworthiness performance" *Electronic Theses and Dissertations*, 2012. p. 114 - 116

[14] A. Ghahremaninezhad and K. Ravi-Chandar, "Ductile failure behavior of polycrystalline Al 6061-T6." *Int. J. Fract. Mech.*, 2012. 174(2): p. 177-202.

[15] A. Ghahremaninezhad and K. Ravi-Chandar, "Ductile failure behavior of polycrystalline Al 6061-T6 under shear dominant loading." *Int. J. Fract. Mech.*, 2013. 180(1): p. 23-39.

[16] D. R. Lesuer, G. Kay, and M. LeBlanc, "Modeling large strain, high rate deformation in metals." *Engineering research, development and technology*, 1999.

[17] F. A. McClintock, "A criterion for ductile fracture by the growth of holes." *J. Appl. Mech.*, 1968. 35(2): p. 363-371.

[18] J. R. Rice and D. M. Tracey, "On the ductile enlargement of voids in triaxial stress fields." *J. Mech. Phys. Solids*, 1969. 17(3): p. 201-217.

[19] A. L. Gurson, "Continuum theory of ductile rupture by void nucleation and growth: Part I—Yield criteria and flow rules for porous ductile media." *J. Eng. Mat. Tech.*, 1977. 99(1): p. 2-15.

[20] C. Chu and A. Needleman, "Void nucleation effects in biaxially stretched sheets." *J. Eng. Mat. Tech.*, 1980. 102(3): p. 249-256.

[21] V. Tvergaard and A. Needleman, "Analysis of the cup-cone fracture in a round tensile bar." *Acta Metall.*, 1984. 32(1): p. 157-169.

[22] Plate bending test for metallic materials, in VDA 238-1002010, *VERBAND DER AUTOMOBILINDUSTRIE E.V.*: Berlin. p. 1-13.

[23] P. Larour, B. Hackl, and F. Leomann, "Sensitivity Analysis on the Calculated Bending Angle in the Instrumented Bending Test." in *IDDRG 2013*. Zurich, Switzerland.

[24] I. Westermann, K. E. Snilsberg, Z. Sharifi, O. S. Hopperstad, K. Marthinsen, B. Holmedal, "Three-point bending of heat-treatable aluminum alloys: influence of microstructure and texture on bendability and fracture behavior." *Metall. Mater. Trans. A.* 2011. 42(11): p. 3386-98.

[25] Parachute. (2015). The Cost of Injury in Canada. *Parachute*: Toronto, ON

[26] ASTM B557: Standard methods of tension testing wrought and cast aluminium and magnesium alloy prducts.*ASTM International*. West Conshohocken, PA.